Phonon anomalies in α-uranium

Xiaodong Yang and Peter S. Riseborough
Physics Department, Temple University, Philadelphia, Pennsylvania 19122, USA
(Received 15 July 2010; revised manuscript received 6 August 2010; published 3 September 2010)

The phonon spectrum of α-uranium has been measured by Manley *et al.* in a series of experiments using inelastic neutron and x-ray scattering. The 2001 results showed that the optic modes soften by a few millielectron volts as the temperature is increased between room temperature and 450 K. In 2006, a new dynamical mode was observed to form above 450 K which the authors attribute to an intrinsically localized mode, which is stabilized by anharmonic interactions. We propose a possible alternate cause for the formation of the mode and the softening which is based on the existence of strong electron-phonon interaction together with a low excitation energy for transitions between states with f and conduction-electron characters. The model allows for a resonant interaction between the optic phonons and the electronic excitations, which may lead to the high-energy peaks in the phonon spectra splitting and acquiring mixed electronic and phonon characters.

DOI: 10.1103/PhysRevB.82.094303 PACS number(s): 63.20.kd, 73.20.Mf

I. INTRODUCTION

Uranium shows indisputable evidence for very strong electron-phonon coupling[1] which is responsible for the material undergoing three structural transformations at low temperatures. The room-temperature phonon-dispersion relations inferred from inelastic neutron-scattering experiments[2] show the existence of a large Kohn anomaly near $q=[0.5,0,0]$ in reciprocal-lattice units. The anomaly has its origin in a weak singularity in the dielectric constant at $q=2k_F$.[3] Although this singularity is extremely weak for isotropic three-dimensional materials, it can be large for systems in which the electronic dispersion relations are extremely anisotropic. From neutron-diffraction data it was found[4,5] that on decreasing temperature new inelastic Bragg peaks first occurred for temperatures below 46 K at points near $[\frac{1}{2},0,0]$ which are not commensurate with the α-phase lattice. Also additional peaks were observed at large wave vectors. Yamada[6] proposed a quasi-one-dimensional theory in which the instability occurs due to Fermi-surface nesting at a wave vector directed along the [1,0,0] axis, and that the extra peaks were consequences of strains induced by domain-wall boundaries. However, it was subsequently found using high-resolution neutron scattering[7] that phonon softening occurred at the exact (temperature-dependent) charge-density wave vectors $Q_c(T)$ off the [1,0,0] axis, and that the square of the soft-mode frequency exhibited a linear variation in $T-T_c$ as expected from the mean-field version of Landau-Ginzberg Theory. The wave vectors Q_c were found to be in perfect agreement with the nesting wave vectors of a fully three-dimensional Fermi surface calculated by Fast *et al.*[8] First-principles calculations of the phonon spectrum by Bouchet[9] show that the Σ_4 mode shows a significant Kohn anomaly at $[\frac{1}{2},0,0]$. The shift of the phonon frequency can be expressed in terms of a product involving the electron-phonon interaction and the linear-response function for electronic excitations. The magnitude of the shift is surprisingly large since only a relatively small portion of the Brillouin zone shows nesting[8] and, furthermore, even in these small regions there is about a 5% variation in the nesting vector. Therefore, the Lindhardt function is not expected to show the $\ln(q_x-Q_c)$ divergence expected from perfectly parallel sheets of the Fermi surface but also, at finite values of (q_x-Q_c), is expected to have a magnitude much smaller than the value of the corresponding one-dimensional function. These findings not only suggest that the lattice instability due to the phonon softening can be thought as a Kohn anomaly produced by the electron-phonon interaction and provides a direct measure of the Fermi-surface nesting[10] but also that the electron-phonon interaction is quite strong.

The thermodynamic properties of α-uranium are also anomalous. The lattice constant shows an unusually large temperature dependence that persists up to room temperatures.[11] Likewise, the magnetic susceptibility, which has been designated as being Pauli paramagnetic,[12] shows an increase with increasing temperature. Taken together, the thermodynamics suggests that there is a low-energy scale for electronic excitations which results in a decrease in bonding and an increase in the magnetic character at elevated temperatures. Therefore, studies of the high-temperature properties could be expected to reveal distinct physics.

The dispersion relation has also been measured at high temperatures ($T\approx 450$ K) by inelastic neutron and x-ray scattering experiments.[13,14] These experiments showed that the optic phonon density of states measured by incoherent inelastic neutron scattering softened by about 4 meV as the temperature was raised from room temperature to 433 K. More surprisingly, further experiments revealed the formation of a dynamical mode with a nontrivial temperature-dependent width.[15] The new mode was observed at 14 meV near the zone boundary at the low-symmetry point (0,1,0.2), where the pre-existing phonon mode at 11 meV was observed to soften. Further experiments[16] have shown that the anomalous mode occurs at a number of low-symmetry points which are related by an approximate hexagonal symmetry of the Brillouin zone. Since the system does not show signs of a structural instability in the temperature range where the new mode forms, the occurrence of the new mode has been heralded as representing a breakdown of harmonic phonon theory, which would predict six phonon modes for a monoclinic lattice with two basis atoms. (The lattice is normally refereed to as orthorhombic with four atoms in the unit cell).

The experimental group attributed the appearance of the new mode to the existence of a thermally activated population of intrinsically localized modes. Loosely speaking, intrinsically localized modes are oscillatory vibrational modes in which the anharmonic interactions restrict the excitations to occur over finite regions of space and which prevent the excitations from dispersing as time evolves. Evidence for such nonlinear excitations were first found by Fermi *et al.*[17] in computer simulations of the vibrational motion of a 33-atom chain in which anharmonic interactions were present. The continuum limit of the Fermi-Pasta-Ulam problem was identified as being governed by the Korteweg-de Vries equation[18] which was shown by Gardner *et al.*[19] to have soliton solutions. Further progress was made by Toda,[20] who found nonlinear excitations in discrete one-dimensional lattices. Flach[21] showed that localized large-amplitude vibrational modes can be considered as quantized bound states of extended small-amplitude waves. Most of the earlier work has been restricted to low-dimensional systems due to Derrick's theorem which predicts that solitonlike modes would become unstable in higher dimensions.[22] Although exact soliton and breather solutions occur frequently for low-dimensional nonlinear systems,[23,24] it has proved to be notoriously difficult to obtain mathematically exact soliton solutions for higher dimensional nonlinear theories. However, the theorem is based on idealized mathematical assumptions and does not preclude the existence of metastable nonlinear localized modes. Hence, as Manley *et al.*[15] argue, intrinsically localized modes might exist in higher dimensions due to "hot spots" and also in discrete lattices which have relatively low point-group symmetries such as α-uranium. The experimental work on α-uranium was followed up by inelastic neutron-scattering experiments on NaI,[25] which showed features consistent with the intrinsically localized modes predicted by classical molecular-dynamics simulations.[26] A thorough discussion of the appearance of intrinsically localized modes in three-dimensional materials, including their effects on the mechanical properties, is given in a recent article by Manley.[27]

At ambient conditions, the electronic structure of α-uranium is reasonably well described by density-functional theory[28,29] which is in qualitative agreement with photoemission[30] and de Haas-van Alphen experiments.[31] However, local-density approximation (LDA) does require some corrections[1] due to moderate correlations given by a GW treatment.[32] As pointed out by Hjelm *et al.*[33] and also by Stojic *et al.*,[34] a modest increase in the unit-cell volume makes α-uranium comparable to plutonium. For the expanded lattice, LDA predicts α-uranium to be magnetic. Likewise, LDA predicts plutonium to be magnetic.[35,36] However, experiments on plutonium have shown that it does not possess a spontaneous magnetic moment,[37] which is probably due to a partial cancellation between the spin and orbital moments[38] and also due to valence fluctuations.[39] Anomalies in the phonon spectrum of plutonium were predicted on the basis of the coupling to low-energy electronic excitations within the dynamical mean-field theory[40] and have subsequently been observed by inelastic x-ray scattering.[41] The properties of the actinide materials, including uranium and plutonium have recently been reviewed buy Moore and van der Laan.[42] Since the α-uranium lattice expands significantly as the temperature increases, one could expect that the moderate many-body effects predicted near $T=0$ should become significantly stronger at temperatures on the order of 450 K. The anomalous phonon spectrum of plutonium motivates the investigation of whether the phonon anomalies observed in the high temperature expanded lattice of α-uranium could also be due to coupling with low-energy electronic excitations. In the next section, we shall present a model for the phonon softening which involves strong electron-phonon coupling and low-energy valence fluctuations.[43,44] In the following section the phonon spectrum will be calculated and then the paper will conclude with a discussion of the results and a comparison with the experimental data.

II. MODEL HAMILTONIAN

The model Hamiltonian is based on the noninteracting Anderson lattice model which describes hybridized $5f$ bands and the conduction bands. The harmonic phonons are coupled to the f electronic system via an electron-phonon interaction. The model was originally introduced by Sherrington *et al.*[45,46] to describe the dynamics of isostructural valence transitions in SmS, where the transition is marked by a discontinuous change in volume caused by the differences in the ionic radii of the Sm ions. The total Hamiltonian is written as

$$\hat{H} = \sum_{i,\sigma} E_f f^\dagger_{i\sigma} f_{i\sigma} + \sum_{\underline{k},\sigma} \epsilon_{\underline{k}} d^\dagger_{\underline{k}\sigma} d_{\underline{k}\sigma} + \sum_{\underline{k},\sigma} (V_{\underline{k}} f^\dagger_{\underline{k}\sigma} d_{\underline{k}\sigma} + V^*_{\underline{k}} d^\dagger_{\underline{k}\sigma} f_{\underline{k}\sigma}) + \sum_{\underline{q},\gamma} \hbar\omega_{\underline{q}\gamma} a^\dagger_{\underline{q}\gamma} a_{\underline{q}\gamma} + \sum_{\underline{k},\sigma,\underline{q},\gamma} \lambda_{\underline{q}\gamma} (a^\dagger_{\underline{q}\gamma} + a_{-\underline{q}\gamma}) f^\dagger_{\underline{k}+\underline{q}\sigma} f_{\underline{k}\sigma}. \quad (1)$$

The first term represents the binding energy E_f of the localized f states at the lattice sites labeled by the index i. Here the operators $f^\dagger_{i\sigma}$ and $f_{i\sigma}$, respectively, create and annihilate an f electron of spin σ in the orbital located at site i. The second term represents the energy $\epsilon_{\underline{k}}$ of the conduction-band Bloch states, labeled by the Bloch wave vector k, and $d^\dagger_{\underline{k}\sigma}$ and $d_{\underline{k}\sigma}$, respectively, create and annihilate a conduction electron of spin σ in the kth Bloch state. The third term represents the hybridization between the localized f electron states and the conduction-band states. The fourth term represents the energy $\hbar\omega_{\underline{q},\gamma}$ of a phonon with wave vector $\underline{q}$ and polarization γ in which $a^\dagger_{\underline{q},\gamma}$ and $a_{\underline{q},\gamma}$ are, respectively, the phonon creation and annihilation operators. The last term represents the interaction between the f electron and the phonons. The order of magnitude of the f electron-phonon coupling strength $\lambda_{\underline{q},\gamma}$ for longitudinal-acoustic phonons is approximated by[47]

$$\lambda_{\underline{q}} = i(\underline{q} \cdot \underline{\epsilon}_{\underline{q}}) \left[\frac{4\pi Z_* e^2}{\Omega_c (q^2 + q^2_{TF})} \right] \sqrt{\frac{\hbar}{2M\omega_{\underline{q}}}}, \quad (2)$$

where $\underline{\epsilon}_{\underline{q}}$ is the polarization vector, Z_* is the charge on the uranium ions ($Z_*=3$), M the nuclear mass ($M=238m_p$), Ω_c is the volume of the unit cell ($\Omega_c=83.2\times10^{-30}$ m^3 for the conventional orthorhombic unit cell), and q_{TF} is the Thomas-

Fermi wave vector. The corresponding expression for the longitudinal-acoustic phonon frequency is given by

$$\omega_q^2 = \frac{16\pi Z_*^2 e^2}{M\Omega_c}\left(\frac{q^2}{q^2+q_{TF}^2}\right). \tag{3}$$

This results in the energy of the longitudinal phonon at $\underline{q}=(0,0,\pi/c)$ to be approximately 18 meV. Although the longitudinal-acoustic and transverse-optic modes do mix slightly yielding a pair of Λ_1 modes, the experimentally determined zone-boundary phonon with an energy of approximately 12 meV does correspond to a longitudinal-acoustic mode. The magnitude of the electron-phonon interaction corresponding to the zone-boundary longitudinal-acoustic mode is found to be approximately 110 meV. A similarly large estimate of the electron-phonon interaction ($\approx$47 meV) can be inferred from consideration of the contraction of the Wigner-Seitz radius along the actinide series, as for example, shown in the paper by Lashley *et al.*[37] These large values could also be anticipated from analysis of the low-temperature phonon softening which gives rise to structural instabilities. In our analysis, we shall find it necessary to use electron-phonon interactions which have magnitudes that are similar to the phonon energies. The conduction-band width W found from the calculations of Chantis *et al.*[32] is estimated to be on the order of 6 eV. The Fermi energy is assumed to lie close to the position of the peak in the density of states of the upper hybridized band. A value of the hybridization matrix element V of about 1/3 eV would be required to obtain reasonable agreement with the density of states at the Fermi energy found from the electronic-structure calculations.

In the limit where the electrons are noninteracting, i.e., $\lambda_{\underline{q},\gamma}=0$, the electronic structure decouples from the phonons. The electronic part of the noninteracting Hamiltonian $\hat{H}_0$ is given by

$$\hat{H}_0 = \sum_{\underline{k},\sigma}(E_f f_{\underline{k}\sigma}^\dagger f_{\underline{k}\sigma} + \epsilon_{\underline{k}} d_{\underline{k}\sigma}^\dagger d_{\underline{k}\sigma} + V_{\underline{k}} f_{\underline{k}\sigma}^\dagger d_{i\sigma} + V_{\underline{k}}^* d_{\underline{k}\sigma}^\dagger f_{\underline{k}\sigma}), \tag{4}$$

which is diagonal in the Bloch index. The phase of the hybridization matrix elements can be gaged away by absorbing the phase in either the d or f electron operators. The noninteracting Hamiltonian can then be diagonalized by introducing a pair of new fermionic operators $\alpha_{\underline{k}}, \beta_{\underline{k}}$, via the canonical transformation

$$\alpha_{\underline{k}\sigma} = f_{\underline{k}\sigma}\cos\Theta_{\underline{k}} + d_{\underline{k}\sigma}\sin\Theta_{\underline{k}},$$

$$\beta_{\underline{k}\sigma} = -f_{\underline{k}\sigma}\sin\Theta_{\underline{k}} + d_{\underline{k}\sigma}\cos\Theta_{\underline{k}}, \tag{5}$$

where $\Theta_{\underline{k}}$ is still to be determined. Since the transformation is canonical, the new fermion operators satisfy the anticommutation relations,

$$\{\alpha_{\underline{k}\sigma}, \alpha_{\underline{k}'\sigma'}^\dagger\}_+ = \delta_{\underline{k}\underline{k}'}\delta_{\sigma,\sigma'},$$

$$\{\beta_{\underline{k}\sigma}, \beta_{\underline{k}'\sigma'}^\dagger\}_+ = \delta_{\underline{k}\underline{k}'}\delta_{\sigma\sigma'},$$

$$\{\alpha_{\underline{k}\sigma}, \beta_{\underline{k}'\sigma'}^\dagger\}_+ = 0. \tag{6}$$

For the choice of $\Theta_{\underline{k}}$ given by

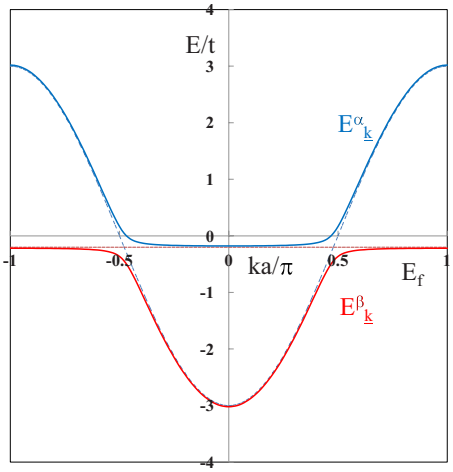

FIG. 1. (Color online) A sketch of the dispersion relations for the hybridized electronic bands.

$$\cos 2\Theta_{\underline{k}} = \frac{E_f - \epsilon_{\underline{k}}}{\sqrt{(E_f-\epsilon_{\underline{k}})^2 + 4V_k^2}},$$

$$\sin 2\Theta_{\underline{k}} = \frac{2V_k}{\sqrt{(E_f-\epsilon_{\underline{k}})^2 + 4V_k^2}}, \tag{7}$$

the terms in the Hamiltonian which are bilinear in the fermion operators α and β vanish. For this choice, the noninteracting electronic Hamiltonian has the diagonal form

$$\hat{H}_0 = \sum_{\underline{k},\sigma}\left(\frac{E_f+\epsilon_{\underline{k}}}{2} + \sqrt{\left(\frac{E_f-\epsilon_{\underline{k}}}{2}\right)^2 + V_k^2}\right)\alpha_{\underline{k}\sigma}^\dagger\alpha_{\underline{k}\sigma}$$
$$+ \sum_{\underline{k},\sigma}\left(\frac{E_f+\epsilon_{\underline{k}}}{2} - \sqrt{\left(\frac{E_f-\epsilon_{\underline{k}}}{2}\right)^2 + V_k^2}\right)\beta_{\underline{k}\sigma}^\dagger\beta_{\underline{k}\sigma}. \tag{8}$$

The electronic dispersion relations are shown in Fig. 1. We note that the spectrum exhibits a direct gap between the pair of hybridized bands of 2 V and an indirect gap given by $\Delta = \frac{4V^2}{W}$, where W is the conduction-band width.

The electron-phonon interaction Hamiltonian $\hat{H}_1$ can be rewritten in terms of the hybridized states as

$$\hat{H}_1 = \frac{1}{\sqrt{N}}\sum_{\underline{k},\underline{q},\sigma,\gamma}\lambda_{\underline{q},\gamma}(a_{\underline{q}\gamma}^\dagger + a_{-\underline{q}\gamma})(\alpha_{\underline{k}\sigma}^\dagger\alpha_{\underline{k}-\underline{q}\sigma}\cos\Theta_{\underline{k}}\cos\Theta_{\underline{k}-\underline{q}}$$
$$+ \beta_{\underline{k}\sigma}^\dagger\beta_{\underline{k}-\underline{q}\sigma}\sin\Theta_{\underline{k}}\sin\Theta_{\underline{k}-\underline{q}} - \alpha_{\underline{k}\sigma}^\dagger\beta_{\underline{k}-\underline{q}\sigma}\cos\Theta_{\underline{k}}\sin\Theta_{\underline{k}-\underline{q}}$$
$$- \beta_{\underline{k}\sigma}^\dagger\alpha_{\underline{k}-\underline{q}\sigma}\sin\Theta_{\underline{k}-\underline{q}}\cos\Theta_{\underline{k}}), \tag{9}$$

where the coherence factors project onto the f states. In the next section, the phonon spectrum will be calculated using a perturbation expansion in the electron-phonon interaction.

III. PHONON SPECTRA

In the absence of interactions, the phonon propagator $D_{\underline{q}\gamma}^0(\omega)$ is diagonal in the polarization indices γ is given by

$$D^0_{q\gamma}(\omega) = \frac{2\hbar\omega_{q\gamma}}{\hbar^2\omega^2 - \hbar^2\omega^2_{q\gamma}}. \tag{10}$$

The propagator for the interacting phonons $D_q(\omega)$ can be expressed in terms of the noninteracting propagator and the irreducible polarization part, $\Pi_q(\omega)$, via Dyson's equation

$$D_q(\omega) = D^0_q(\omega) + D^0_q(\omega)\Pi_q(\omega)D_q(\omega). \tag{11}$$

To lowest order in the electron-phonon interaction, the irreducible polarization part is given by

$$\Pi_q(\omega) = \frac{\hbar}{N}\sum_{k,\sigma}\int \frac{d\omega'}{2\pi i}|\lambda_{q,\gamma}|^2 G^0_{k+q,f}(\omega'+\omega)G^0_{k,f}(\omega'), \tag{12}$$

where $G^0_{k,f}(\omega)$ is the noninteracting single-particle f-electron Green's function. On evaluating the integrations, one obtains the real part of the polarization part as

$$\begin{aligned}\mathrm{Re}\,\Pi_q(\omega) = \frac{2\lambda^2_{q,\gamma}}{N}\sum_k \Bigg[& \frac{(f^\alpha_k - f^\alpha_{k+q})\cos^2\Theta_k \cos^2\Theta_{k+q}}{\hbar\omega + E^\alpha_k - E^\alpha_{k+q}} \\ & + \frac{(f^\beta_k - f^\beta_{k+q})\sin^2\Theta_k \sin^2\Theta_{k+q}}{\hbar\omega + E^\beta_k - E^\beta_{k+q}} \\ & + \frac{(f^\beta_k - f^\alpha_{k+q})\sin^2\Theta_k \cos^2\Theta_{k+q}}{\hbar\omega + E^\beta_k - E^\alpha_{k+q}} \\ & + \frac{(f^\alpha_k - f^\beta_{k+q})\cos^2\Theta_k \sin^2\Theta_{k+q}}{\hbar\omega + E^\alpha_k - E^\beta_{k+q}} \Bigg],\end{aligned} \tag{13}$$

where f^α_k is the Fermi-Dirac distribution function for the kth Bloch state of the α hybridized electronic band. The imaginary part of the polarization part is given by

$$\begin{aligned}\mathrm{Im}\,\Pi_q(\omega + i\eta) = -\frac{2\pi\lambda^2_{q,\gamma}}{N}\sum_k [& \delta(\hbar\omega + E^\alpha_k - E^\alpha_{k+q})(f^\alpha_k \\ & - f^\alpha_{k+q})\cos^2\Theta_k \cos^2\Theta_{k+q} + \delta(\hbar\omega + E^\beta_k \\ & - E^\beta_{k+q})(f^\beta_k - f^\beta_{k+q})\sin^2\Theta_k \sin^2\Theta_{k+q} + \delta(\hbar\omega \\ & + E^\beta_k - E^\alpha_{k+q})(f^\beta_k - f^\alpha_{k+q})\sin^2\Theta_k \cos^2\Theta_{k+q} \\ & + \delta(\hbar\omega + E^\alpha_k - E^\beta_{k+q})(f^\alpha_k \\ & - f^\beta_{k+q})\cos^2\Theta_k \sin^2\Theta_{k+q}].\end{aligned} \tag{14}$$

The real part and imaginary part are connected by the Kramers-Krönig relations

$$\mathrm{Re}\,\Pi_q(\omega) = \frac{1}{\pi}\int_{-\infty}^{+\infty} d\omega' \frac{\mathrm{Im}\,\Pi_q(\omega' + i\eta)}{\omega' - \omega} \tag{15}$$

and

$$\mathrm{Im}\,\Pi_q(\omega + i\eta) = -\frac{Pr}{\pi}\int_{-\infty}^{+\infty} d\omega' \frac{\mathrm{Re}\,\Pi_q(\omega')}{\omega' - \omega - i\eta}, \tag{16}$$

which expresses causality. The polarization part satisfies symmetry relations. In particular, due to time-reversal invariance, the real part is an even function of ω and imaginary part is an odd function of ω.

To lowest order in the electron-phonon interaction, the renormalized phonon and decay rates frequencies are determined by the complex poles of the approximate phonon propagator

$$D_q(\omega) = \frac{2\hbar\omega_q}{\hbar^2\omega^2 - \hbar^2\omega^2_q - 2\hbar\omega_q\Pi_q(\omega)}, \tag{17}$$

which omits the couplings between the various phonon modes. This yields the equation

$$\hbar^2\omega^2 - \hbar^2\omega^2_q - 2\hbar\omega_q\Pi_q(\omega) = 0, \tag{18}$$

which is to be solved graphically. The real parts of the phonon frequencies are approximately given by the intersection of the curves $\omega^2 - \omega^2_q$ and $2\omega_q\,\mathrm{Re}\,\Pi_q(\omega)$, and the phonon decay rates are given by $\mathrm{Im}\,\Pi_q(\omega + i\eta)$ at the intersection.

The form of the frequency-dependent polarization part is shown in Fig. 2 for the values of $q=(0,0,0)$ and $q=(\pi,\pi,\pi)$. For these particular q values, the intraband scattering processes do not contribute to the polarization part in the energy range of interest. The low-energy intraband contributions are restricted to a range of small but finite q and give rise to the structures seen in Fig. 3. The intraband contributions are unlikely to yield phonon anomalies since one expects that Fermi velocity will be much greater than the speed of sound, so the Born-Oppenheimer approximation applies. For $q=(0,0,0)$ the intraband contributions to the polarization part vanish identically when $\omega \neq 0$ and the polarization part, shown in the left panel of Fig. 2, is dominated by the interband contributions. The interband processes exhibits a sharp peak at the threshold energy of $2V$ which corresponds to the direct gap. Since $2V$ is much larger than the phonon energy scale, the renormalizations of the phonon frequencies are expected to be minimal at $q=(0,0,0)$. On the other hand, for $q=(\pi,\pi,\pi)$ the threshold for the interband excitations will be on the order of the much smaller indirect-gap energy $\Delta = 4V^2/W$, as can be seen in the right panel of Fig. 2.

When the threshold for interband excitations is greater than the bare phonon frequency, the polarization part has the effect of reducing the phonon frequency. The softening increases when the separation between the bare phonon frequency and the indirect gap is reduced. When the threshold energy is comparable to the optic phonon frequency, then the low-energy electronic excitations can resonate with the optic phonons leading to the formation of modes of mixed electronic and phononic character. In particular, for phonons with bare frequencies slightly above the interband threshold, the phonon spectral density may show two features: a narrow feature with energies below the threshold and a broader structure located above the threshold but below the bare pho-

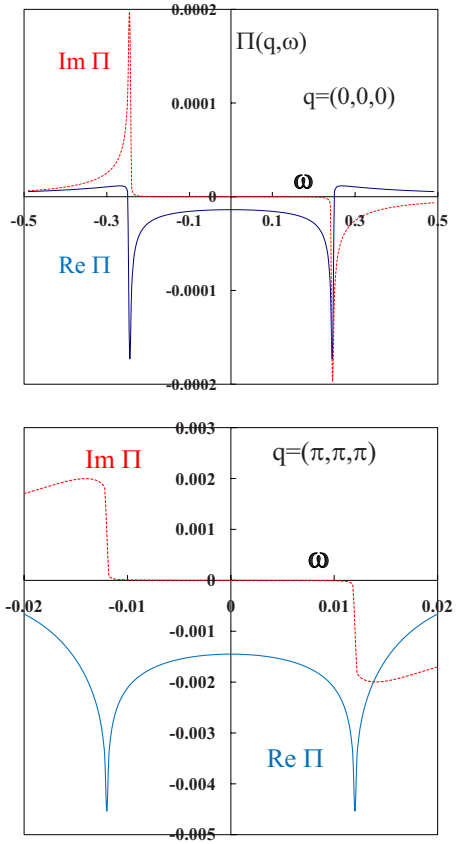

FIG. 2. (Color online) The upper panel shows the frequency dependence of the polarization part for $q=(0,0,0)$. The real part is symmetric in frequency (solid blue line) and imaginary part is odd (dashed red line). The polarization part shows structure at the energy of the direct gap $2V$. The lower panel shows the corresponding polarization part for $q=(\pi,\pi,\pi)$. The polarization part shows structure at the threshold for interband transitions. This threshold is related to the indirect gap Δ. The slight shift is caused by the chemical potential μ which is positioned at an energy of 6 meV in the upper hybridized band. Note the different scales in the two panels.

non frequency which represents the resonance. The graphical solution and the phonon spectral density are shown in Fig. 4. The ω-integrated intensity of the lower mode is given by the expression

$$\left[1-\frac{\partial}{\partial\hbar\omega}\Pi_{\underline{q}}(\omega)\right]^{-1}, \tag{19}$$

which should be reduced below unity. The intrinsic width of the mode due to anharmonic interactions (not considered here) should be reduced by the same factor. The two solutions may be designated as breathing modes which involve the phonons coupling coherently with f-d charge fluctuations and the concomitant change in ionic radii. The model shows that this resonance should only occur for the higher frequency optic modes, and then only for a limited range of large q values for which the threshold energy for interband electronic excitations is reduced below the bare phonon frequency. This finding is qualitatively in agreement with the experimentally results of Manley *et al.*[15] which show that the

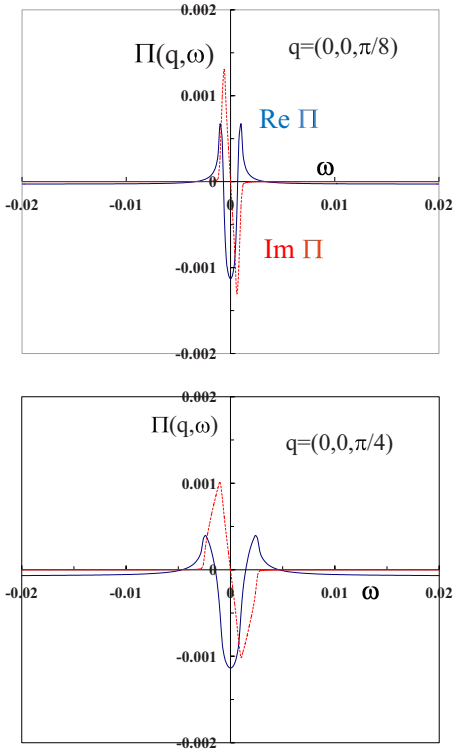

FIG. 3. (Color online) The upper panel shows the low-frequency variation in the polarization part for $q=(0,0,\pi/8)$. The real part is symmetric in frequency (solid blue line) and imaginary part is odd (dashed red line). The lower panel shows the corresponding polarization part for $q=(0,0,\pi/4)$. For this range of momenta and frequencies, the polarization part is dominated by the intraband contribution and resembles the Lindhardt function for electrons with renormalized masses.

new mode is found predominantly near the Y point at the Brillouin-zone boundary. If the phonon frequency is further increased above the electronic threshold, the high-energy resonance may eventually turn into a bound state. For further increases in the phonon frequency, the lower mode may rapidly lose intensity and merge with the continuum. In such cases, the lower mode has an energy ω below the indirect-gap energy Δ which is approximately given by

$$\hbar\omega \approx \Delta\left(1-\exp\left[-\frac{\Delta(\hbar^2\omega_q^2-\Delta^2)}{\lambda_q^2\hbar\omega_q}\right]\right) \tag{20}$$

and the ω-integrated intensity should show an exponential fall off. On further increase in the phonon frequency or weakening of the electron-phonon interaction, the lower mode may have a protracted existence as a narrow resonance as seen in Fig. 5.

IV. DISCUSSION

The major assumption of the above analysis is that there exist low-energy electronic excitations which have energies comparable to those of the optic phonon modes. Since the electronic energy scales derived from first-principles calculations[32] at ambient conditions are about a factor of 10

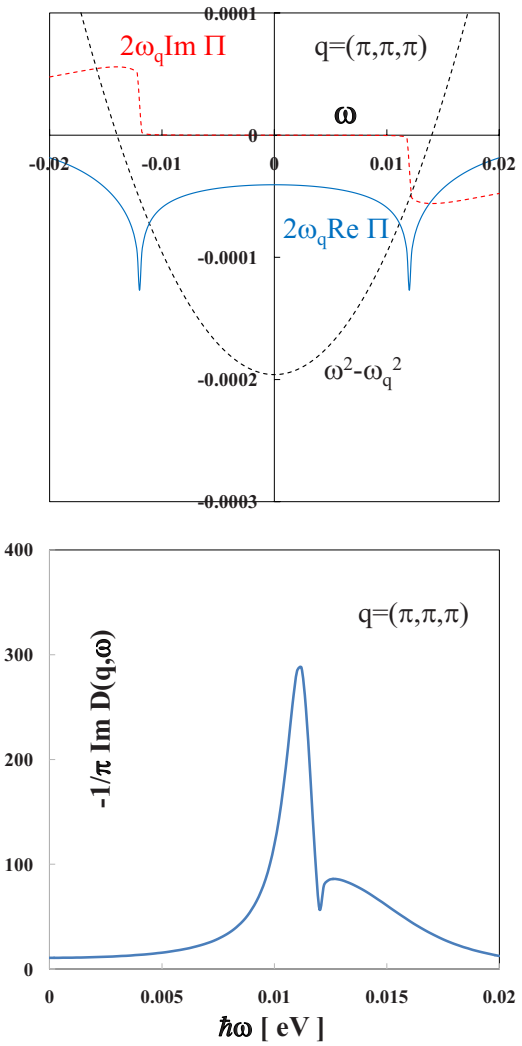

FIG. 4. (Color online) The upper panel shows the graphical solution for the renormalized phonon frequency. The renormalized phonon frequency is given by the intersection of the line $2\omega_q\Pi_q(\omega)$ (solid blue line) with the parabola $\omega^2-\omega_q^2$ (dashed black line). The plot shows that the renormalized phonon frequency exhibits a significant softening when the bare frequency is comparable to the threshold energy Δ. The lower panel shows the phonon spectral density. It shows the softened phonon line at lower frequencies and the formation of resonance mode of mixed electron and phonon character at higher frequencies. A constant has been added to the phonon linewidths to simulate the contributions from anharmonic processes.

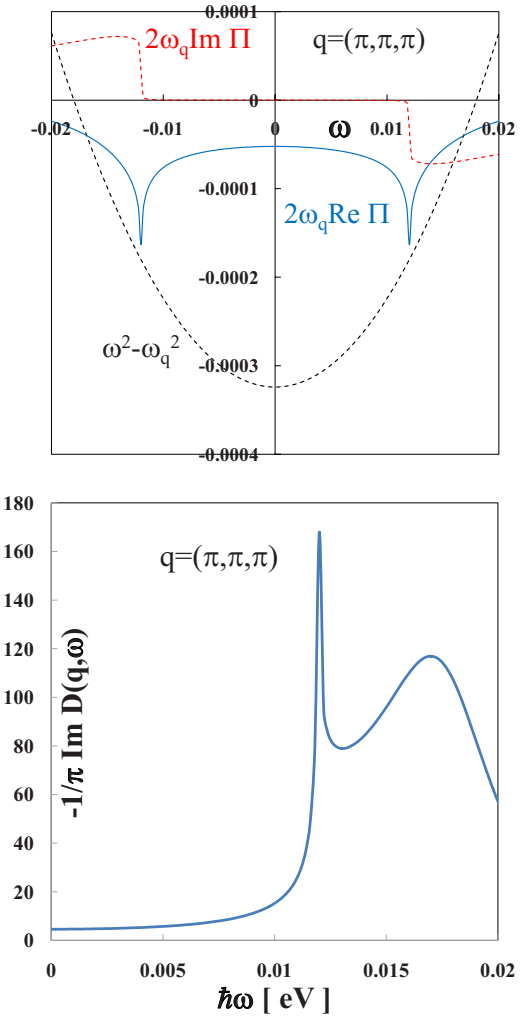

FIG. 5. (Color online) The upper panel shows the graphical solution for the renormalized phonon frequency. This figure differs from Fig. 5 in that the value of the bare phonon frequency has been increased slightly. The renormalized phonon frequency is given by the intersection of the line $2\omega_q\Pi_q(\omega)$ (solid blue line) with the parabola $\omega^2-\omega_q^2$ (dashed black line). The plot shows that although the renormalized phonon frequency lies above the threshold energy Δ, the separation of the curves still shows a local minimum near Δ which may allow the lower frequency mode to exist as a resonance. The lower panel shows the phonon spectral density. It shows that in this case, a narrow resonance exists near the threshold energy. A constant has been added to the phonon linewidths to simulate the contributions from anharmonic processes.

larger than those required for the formation of the breathing mode, the postulated reduction requires a many-body explanation. One possibility is that the reduction in scale is due to the Kondo effect or low-energy valence fluctuations[39] as has been used[40] to predict the experimentally determined phonon anomalies in plutonium.[41] A second possibility, namely, that the reduction is due to a polaronic effect is outlined below.

The first occurrence of the split phonon modes at high temperatures can be understood if one assumes that the hybridization energy is subject to a polaronic reduction. This can be achieved by using a canonical transformation which is a variant of the Lee-Low-Pines transformation[48] and is given by

$$\hat{U}=\exp\left[-\frac{1}{\sqrt{N}}\sum_{\underline{q},j,\sigma,\gamma}\frac{\lambda_{q,\gamma}}{\hbar\omega_{\underline{q},\gamma}}(a^{\dagger}_{\underline{q},\gamma}-a_{-\underline{q},\gamma})f^{\dagger}_{j,\sigma}f_{j,\sigma}\exp(i\underline{q}\cdot\underline{R}_j)\right]. \tag{21}$$

Applying the transformation to the parts of the Hamiltonian which couple to the phonons, one can eliminate the electron-phonon interaction since

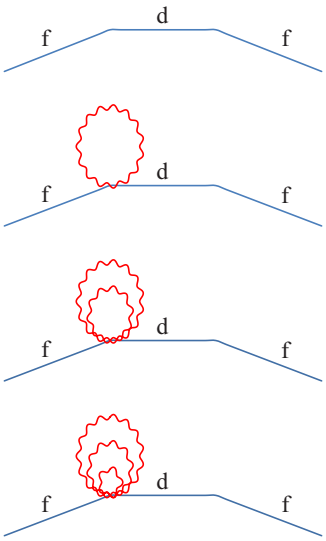

FIG. 6. (Color online) The series of simultaneous emission and absorption of phonons at a hybridization vertex which leads to a polaronic reduction in the hybridization matrix element. The solid blue lines represent the noninteracting one-electron Green's function and the red wavy lines represent the phonon propagators.

$$\hat{H}'_{ph} = \hat{U}^{\dagger}\left[\sum_{\underline{q}\gamma} \hbar\omega_{\underline{q}\gamma} a^{\dagger}_{\underline{q}\gamma} a_{\underline{q}\gamma} + \frac{1}{\sqrt{N}} \sum_{\underline{q},\underline{k}\gamma} \lambda_{\underline{q}\gamma} (a^{\dagger}_{\underline{q}\gamma} + a_{-\underline{q}\gamma}) f^{\dagger}_{\underline{k}} f_{\underline{k}-\underline{q}}\right]\hat{U}$$

$$= \sum_{\underline{q},\gamma} \hbar\omega_{\underline{q}\gamma} a^{\dagger}_{\underline{q}\gamma} a_{\underline{q}\gamma} - \frac{1}{N} \sum_{\underline{q},\underline{k},\underline{k}'} \frac{\lambda^2_{\underline{q}\gamma}}{\hbar\omega_{\underline{q}\gamma}} f^{\dagger}_{\underline{k}-\underline{q}} f_{\underline{k}} f^{\dagger}_{\underline{k}'+\underline{q}} f_{\underline{k}'}. \quad (22)$$

Thus, the Hamiltonian is diagonal in the limit $V \to 0$ in which case, the linear electron-phonon coupling is removed but in the process, produces a Frank-Condon shift of the f level and also produces an oscillatory long-ranged interaction between the f electrons.[45,46] The canonical transformation has the effect of producing a dynamic renormalization of the hybridization term to yield

$$H'_V = \sum_{j,\underline{k},\gamma} \left\{ V \exp[i\underline{k}\cdot\underline{R}_j] f^{\dagger}_{j,\alpha} d_{\underline{k},\alpha} \exp\left[-\frac{1}{\sqrt{N}} \sum_{\underline{q},\gamma} \frac{\lambda_{q,\gamma}}{\hbar\omega_{\underline{q},\gamma}} (a^{\dagger}_{\underline{q},\gamma} - a_{-\underline{q},\gamma}) \exp(i\underline{q}\cdot\underline{R}_j) \right] + \text{H.c.} \right\}. \quad (23)$$

If this is replaced by the thermal average, as in the Gutzwiller approximate treatment of electronic correlations, one recovers a polaronic reduction in the effective hybridization interaction of the form

$$V \to \tilde{V} = V \exp\left\{ -\frac{1}{2N} \sum_{\underline{q},\gamma} \left(\frac{\lambda_{q,\gamma}}{\hbar\omega_{\underline{q},\gamma}} \right)^2 [1 + 2N(\omega_{\underline{q},\gamma})] \right\}. \quad (24)$$

Diagrammatically, this corresponds to the simultaneous emission and absorption of an indefinite number of phonons at the hybridization vertex, as indicated by the infinite series depicted in Fig. 6. The temperature dependence of the renormalized hybridization matrix element is similar to that found in Holstein's treatment of the small polaron.[49] It is hypothesized that the temperature-dependent renormalization of the hybridization matrix element, and the concomitant reduction in the indirect hybridization gap, is responsible for the occurrence of the breathing mode at high temperatures. This polaronic renormalization only occurs for the low-energy f quasiparticles. The higher energy excitations are unrenormalized, as is indicated below. For moderately large polaronic reductions, one might expect that the f-electron self-energy could be calculated to leading orders in $\tilde{V}^2$, and that the dynamic part of the hybridization might also be expanded in powers of $(\frac{\lambda_{q,\gamma}}{\hbar\omega_{q\gamma}})^2$. To lowest nontrivial order in the effective hybridization, the self-energy for the fermionic part of the transformed f electron Green's function can be expanded in powers of the dynamic electron-phonon coupling as depicted in Fig. 7. This yields the expression

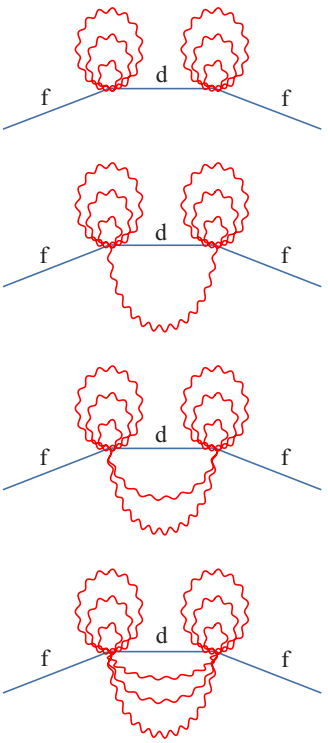

FIG. 7. (Color online) The self-energy for the f quasiparticle Green's function corresponding to the series of emission and absorption of phonons propagating between two adjacent polaronically renormalized hybridization vertices. The symbols are the same as in Fig. 6.

$$\Sigma_f(\underline{k},\omega) \approx |\tilde{V}|^2 \left\{ \frac{1}{\hbar\omega - \epsilon_{\underline{k}} + \mu} + \frac{1}{N} \sum_{\underline{q},\gamma} \left(\frac{\lambda_{q,\gamma}}{\hbar\omega_{\underline{q},\gamma}} \right)^2 \left[\frac{1 + N(\omega_{q,\gamma}) - f_{\underline{k}-\underline{q}}}{\hbar\omega - \epsilon_{\underline{k}-\underline{q}} + \mu - \hbar\omega_{\underline{q},\gamma}} + \frac{N(\omega_{q,\gamma}) + f_{\underline{k}-\underline{q}}}{\hbar\omega - \epsilon_{\underline{k}-\underline{q}} + \mu + \hbar\omega_{\underline{q},\gamma}} \right] + \cdots \right\}. \quad (25)$$

The first term in the above expansion produces a highly renormalized branch of quasiparticle excitations close to the Fermi energy. However, at excitation energies greater than $\hbar\omega_D$ from the Fermi surface, the quasiparticle excitations becomes unrenormalized as can be inferred by expanding the second and third terms in powers of $\omega_{q\gamma}$, yielding

$$\Sigma_f(k,\omega) \approx |\tilde{V}|^2 \Bigg\{ \frac{1}{\hbar\omega - \epsilon_{\underline{k}} + \mu} + \frac{1}{N}\sum_{\underline{q},\gamma} \left(\frac{\lambda_{q,\gamma}}{\hbar\omega_{\underline{q},\gamma}} \right)^2 \times \left[\frac{1 + 2N(\omega_{q,\gamma})}{\hbar\omega - \epsilon_{\underline{k}-\underline{q}} + \mu} \right] + \frac{1}{N}\sum_{\underline{q},\gamma} \left(\frac{\lambda_{q,\gamma}}{\hbar\omega_{\underline{q},\gamma}} \right)^2 \times \hbar\omega_{q,\gamma} \left[\frac{1 - 2f_{\underline{k}-q}}{(\hbar\omega - \epsilon_{\underline{k}-\underline{q}} + \mu)^2} \right] + \cdots \Bigg\}. \tag{26}$$

For energies removed from the Fermi energy (so the denominators are far from resonance), it can be inferred that the second term represents the lowest-order term of the series which has the effect of removing the polaronic reduction in the square of the effective hybridization matrix elements

$$|V|^2 \approx |V|^2 \exp\left\{ -\frac{1}{N}\sum_{\underline{q},\gamma} \left(\frac{\lambda_{q,\gamma}}{\hbar\omega_{\underline{q},\gamma}} \right)^2 [1 + 2N(\omega_{\underline{q},\gamma})] \right\} \times \left\{ 1 + \frac{1}{N}\sum_{\underline{q},\gamma} \left(\frac{\lambda_{q,\gamma}}{\hbar\omega_{\underline{q},\gamma}} \right)^2 [1 + 2N(\omega_{\underline{q},\gamma})] + \cdots \right\}. \tag{27}$$

This leads to the overall f density of states being unrenormalized by the electron-phonon coupling.

The low-energy contribution to the irreducible polarization part is given by the quasiparticle contribution shown in Fig. 8, which has the leading-order contribution given by

$$\Pi_{\underline{q}}(\omega) = \frac{2}{N}\left(\frac{\tilde{V}\lambda_{q,\gamma}}{\hbar\omega_{\underline{q}\gamma}} \right)^2 \sum_{\underline{k}} \Bigg[\frac{(f^{\alpha}_{\underline{k}} - f^{\alpha}_{\underline{k}+q})\sin^2\Theta_{\underline{k}}\cos^2\Theta_{\underline{k}+q}}{\hbar\omega + E^{\alpha}_{\underline{k}} - E^{\alpha}_{\underline{k}+\underline{q}}} + \frac{(f^{\beta}_{\underline{k}} - f^{\beta}_{\underline{k}+q})\cos^2\Theta_{\underline{k}}\sin^2\Theta_{\underline{k}+q}}{\hbar\omega + E^{\beta}_{\underline{k}} - E^{\beta}_{\underline{k}+q}} + \frac{(f^{\beta}_{\underline{k}} - f^{\alpha}_{\underline{k}+q})\cos^2\Theta_{\underline{k}}\cos^2\Theta_{\underline{k}+q}}{\hbar\omega + E^{\beta}_{\underline{k}} - E^{\alpha}_{\underline{k}+\underline{q}}} + \frac{(f^{\alpha}_{\underline{k}} - f^{\beta}_{\underline{k}+q})\sin^2\Theta_{\underline{k}}\sin^2\Theta_{\underline{k}+q}}{\hbar\omega + E^{\alpha}_{\underline{k}} - E^{\beta}_{\underline{k}+\underline{q}}} \Bigg] \tag{28}$$

in which all terms involve the polaronically renormalized hybridization matrix element $\tilde{V}$. This has the same energetic structure as that considered previously, although the intensities differ. The polaronically renormalized indirect gap is expected to decrease with increasing temperatures. Initially, it is expected that this reduction will have the effect of producing an increase in the magnitude of the polarization part

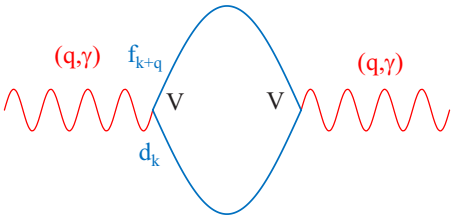

FIG. 8. (Color online) The lowest-order contribution to the phonon polarization part, in the transformed representation. For clarity, the polaronic renormalizations of the hybridization vertices $\tilde{V}$ are not shown. The symbols are the same as in Fig. 6.

(evaluated at the bare phonon frequency) as the temperature increases. This results in an initial softening of the optic phonon modes with increasing temperature, consistent with the experimental findings of Manley *et al.*[13] The polaronic reduction in the indirect gap also yields the result that the breathing modes only forms at sufficiently high temperatures, at which the indirect gap becomes comparable to the optic phonon energy. Furthermore, these breathing modes are only expected to exist over a limited range of temperatures since for sufficiently high temperatures the effective strength of the electron-phonon coupling interaction given by

$$\frac{\tilde{V}\lambda_{q,\gamma}}{\hbar\omega_{\underline{q},\gamma}} \tag{29}$$

will be reduced below the critical strength necessary to cause the resonance to split the modes.

In summary, we have presented a model to describe the phonon anomalies in α-uranium that is an alternative to the intrinsically localized mode description. In particular, we have shown that when the f-d electronic excitation energies are comparable to the optic phonon frequencies, strong f-electron-phonon coupling can cause the phonon frequencies to soften and in a critical range may cause the phonon modes to become resonant and split forming breathing modes of mixed electron-phonon characters. These modes will only occur for a limited range of q values and are restricted to the higher energy portions of the unrenormalized phonon spectra. Furthermore, we have indicated how the observed temperature-dependent softening of the optic phonon frequencies and the evolution of the new mode can be reconciled with this theory, if one assumes the existence of a significant polaronic renormalization of the quasiparticle excitations.

ACKNOWLEDGMENTS

This work was supported by a grant from the U.S. Department of Energy, Office of Basic Energy Sciences through Award No. DEFG02-84ER45872. The authors would also like to acknowledge stimulating conversations with G. H. Lander, J. C. Lashley, M. E. Manley, J. L. Smith, and J. Tobin.

[1] G. H. Lander, E. S. Fisher, and S. D. Bader, Adv. Phys. **43**, 1 (1994).
[2] W. P. Crummett, H. G. Smith, R. M. Nicklow, and N. Wakabayashi, Phys. Rev. B **19**, 6028 (1979).
[3] W. Kohn, Phys. Rev. Lett. **2**, 393 (1959).
[4] H. G. Smith, N. Wakabayashi, W. P. Crummett, R. M. Nicklow, G. H. Lander, and E. S. Fisher, Phys. Rev. Lett. **44**, 1612 (1980).
[5] G. H. Lander, E. S. Fisher, N. Wakabayashi, W. P. Crummett, and R. M. Nicklow, Physica B & C **102**, 326 (1980).
[6] Y. Yamada, Phys. Rev. B **47**, 5614 (1993).
[7] J. C. Marmeggi, R. Currat, A. Bouvet, and G. H. Lander, Physica B **263-264**, 624 (1999).
[8] L. Fast, O. Eriksson, B. Johansson, J. M. Wills, G. Straub, H. Roeder, and L. Nordstrom, Phys. Rev. Lett. **81**, 2978 (1998).
[9] J. Bouchet, Phys. Rev. B **77**, 024113 (2008).
[10] J. C. Marmeggi, R. Currat, A. Bouvet, and G. H. Lander, Physica B **276-278**, 272 (2000).
[11] C. S. Barrett, M. H. Mueller, and R. L. Hitterman, Phys. Rev. **129**, 625 (1963).
[12] J. W. Ross and D. J. Lam, Phys. Rev. **165**, 617 (1968).
[13] M. E. Manley, B. Fultz, R. J. McQueeney, C. M. Brown, W. L. Hults, J. L. Smith, D. J. Thoma, R. Osborn, and J. L. Robertson, Phys. Rev. Lett. **86**, 3076 (2001).
[14] M. E. Manley, G. H. Lander, H. Sinn, A. Alatas, W. L. Hults, R. J. McQueeney, J. L. Smith, and J. Willit, Phys. Rev. B **67**, 052302 (2003).
[15] M. E. Manley, M. Yethiraj, H. Sinn, H. M. Volz, A. Alatas, J. C. Lashley, W. L. Hults, G. H. Lander, and J. L. Smith, Phys. Rev. Lett. **96**, 125501 (2006).
[16] M. E. Manley, J. W. Lynn, Y. Chen, and G. H. Lander, Phys. Rev. B **77**, 052301 (2008).
[17] E. Fermi, J. Pasta, and S. Ulam, Los Alamos Report No. LA-1940, May 1955 (unpublished).
[18] D. J. Korteweg and G. de Vries, Philos. Mag. **39**, 422 (1895).
[19] C. S. Gardner, J. M. Greene, M. D. Kruskal, and R. M. Muira, Phys. Rev. Lett. **19**, 1095 (1967).
[20] M. Toda, J. Phys. Soc. Jpn. **22**, 431 (1967); M. Toda and M. Wati, *ibid.* **34**, 18 (1973).
[21] S. Flach, Phys. Rev. E **50**, 3134 (1994).
[22] G. H. Derrick, J. Math. Phys. **5**, 1252 (1964).
[23] K. M. Leung, D. W. Hone, D. L. Mills, P. S. Riseborough, and S. E. Trullinger, Phys. Rev. B **21**, 4017 (1980).
[24] P. S. Riseborough and S. E. Trullinger, Phys. Rev. B **22**, 4389 (1980).
[25] M. E. Manley, A. J. Sievers, J. W. Lynn, S. A. Kiselev, N. I. Agladze, Y. Chen, A. Llobet, and A. Alatas, Phys. Rev. B **79**, 134304 (2009).
[26] S. A. Kiselev and A. J. Sievers, Phys. Rev. B **55**, 5755 (1997).
[27] M. E. Manley, Acta Mater. **58**, 2926 (2010).
[28] H. L. Skriver and I. Mertig, Phys. Rev. B **32**, 4431 (1985).
[29] J. M. Wills and O. Eriksson, Phys. Rev. B **45**, 13879 (1992).
[30] C. P. Opeil, R. K. Schulze, M. E. Manley, J. C. Lashley, W. L. Hults, R. J. Hanrahan, Jr., J. L. Smith, B. Mihaila, K. B. Blagoev, R. C. Albers, and P. B. Littlewood, Phys. Rev. B **73**, 165109 (2006).
[31] D. Graf, R. Stillwell, T. P. Murphy, J.-H. Park, M. Kano, E. C. Palm, P. Schlottmann, J. Bourg, K. N. Collar, J. C. Cooley, J. C. Lashley, J. Willit, and S. W. Tozer, Phys. Rev. B **80**, 241101 (2009).
[32] A. N. Chantis, R. C. Albers, M. D. Jones, M. van Schilfgaarde, and T. Kotani, Phys. Rev. B **78**, 081101 (2008).
[33] A. Hjelm, O. Eriksson, and B. Johansson, Phys. Rev. Lett. **71**, 1459 (1993).
[34] N. Stojić, J. W. Davenport, M. Komelj, and J. Glimm, Phys. Rev. B **68**, 094407 (2003).
[35] G. Schadler, P. Weinberger, A. M. Boring, and R. C. Albers, Phys. Rev. B **34**, 713 (1986).
[36] I. V. Solovyev, A. I. Liechtenstein, V. A. Gubanov, V. P. Antropov, and O. K. Andersen, Phys. Rev. B **43**, 14414 (1991).
[37] J. C. Lashley, A. Lawson, R. J. McQueeney, and G. H. Lander, Phys. Rev. B **72**, 054416 (2005).
[38] P. Söderlind, Europhys. Lett. **55**, 525 (2001).
[39] S. Y. Savrasov, G. Kotliar, and E. Abrahams, Nature (London) **410**, 793 (2001).
[40] X. Dai, S. Y. Savrasov, G. Kotliar, A. Migliori, H. Ledbetter, and E. Abrahams, Science **300**, 953 (2003).
[41] J. Wong, M. Krisch, D. L. Farber, F. Occelli, A. J. Schwartz, T.-C. Chiang, M. Wall, C. Boro, and R. Xu, Science **301**, 1078 (2003).
[42] K. S. Moore and G. van der Laan, Rev. Mod. Phys. **81**, 235 (2009).
[43] N. Grewe, P. Entel, and H. J. Leder, Z. Phys. B: Condens. Matter **30**, 393 (1978).
[44] P. S. Riseborough and X. Yang, J. Magn. Magn. Mater. **310**, 938 (2007).
[45] D. Sherrington and P. S. Riseborough, J. Phys. Colloq. **37**, C4-255 (1976).
[46] D. Sherrington and S. von Molnar, Solid State Commun. **16**, 1347 (1975).
[47] J. Bardeen and D. Pines, Phys. Rev. **99**, 1140 (1955).
[48] T. D. Lee, F. E. Low, and D. Pines, Phys. Rev. **90**, 297 (1953).
[49] T. Holstein, Ann. Phys. (N.Y.) **8**, 325 (1959) **8**, 343 (1959).